# $^1$H NMR Spectroscopic and Quantum Chemical Studies on a Poly(ester amide) Model Compound: $N_\alpha$-Benzoyl-L-Argininate Ethyl Ester Chloride. Structural Preferences for the Isolated Molecule and in Solution

**A. C. Fonseca,[†] S. Jarmelo,[†,‡] R. A. Carvalho,[§] R. Fausto,[‡] M. H. Gil,[†] and P. N. Simões*[,†]**

*Department of Chemical Engineering, University of Coimbra, Pólo II, Pinhal de Marrocos, 3030-790 Coimbra, Portugal, Department of Chemistry, University of Coimbra, 3004-535 Coimbra, Portugal, and Department of Life Sciences and Center for Neurosciences, University of Coimbra, 3001-401 Coimbra, Portugal*

*Received: December 3, 2009; Revised Manuscript Received: April 5, 2010*

The molecular structure of the L-arginine derivative, $N_\alpha$-benzoyl-L-argininate ethyl ester chloride ($BAEEH^+ \cdot Cl^-$), was characterized by combining quantum chemical methods and $^1$H NMR spectroscopy. A conformational search on the potential energy surfaces of the three lowest-energy tautomers of $BAEEH^+$ [**A**: R−$N^+$H═$(NH_2)_2$; **B**: R−NH−C(═NH)$N^+H_3$; **C**: R−$N^+H_2$−C(═NH)$NH_2$; R = $C_6H_5$C(═O)NH−CH($COOCH_2CH_3$)$CH_2CH_2CH_2$−] was carried out using the semiempirical PM3 method. The lowest-energy conformations obtained using this method were then optimized at the DFT(B3LYP)/6-31++G(d,p) level of theory. For all tautomers, it was found that all low-energy conformers present folded structures, in which a H-bond interaction between the guanidinium group and the amide carbonyl oxygen atom appears to be the most relevant stabilizing factor. $^1$H NMR spectra of $BAEEH^+ \cdot Cl^-$ in DMF-$D_7$ were acquired in the temperature range [−55 to 75 °C], providing information about the rotational motions in the guanidinium group and showing that the tautomeric form of $BAEEH^+$ that exists in solution is tautomer **A**. The interpretation of the experimental findings was supported by $^1$H NMR chemical shifts obtained theoretically at the DFT(B3LYP)/6-31++G(d,p) level of approximation, using both the polarized continuum model and a $BAEEH^+$−water complex model.

## Introduction

In the past years, there has been an increasing interest in developing new biocompatible and biodegradable materials with controlled lifetimes for biomedical applications.[1,2]

Polyesters, like poly(lactic acid) (PLA) or poly(glycolic acid) (PGA) and their copolymers, have been extensively used in the biomedical field (e.g. sutures, drug delivery systems, or scaffolds for tissue engineering) due to their low immunogenicity and good biocompatibility.[1,3] However, the interaction between these polymers and cells is poor, due to the absence of lateral reactive groups, which may promote specific and desirable interactions between cells and polymer. A possible strategy to overcome this limitation is the incorporation of versatile functional groups in the structure of the polymer, such as amino (−$NH_2$) or hydroxyl (−OH) moieties.

Poly(ester amide)s (PEAs), presenting amide (−CONH−) and ester (−COO−) groups in their chain, emerged as an important class of biocompatible and biodegradable materials with potential applications in the fields mentioned above.[4,5] From the point of view of pharmaceutical and biomedical applications, these materials represent particularly promising systems since they have the ability to establish strong biospecific intermolecular H-bond interactions (through their amide groups) with cell components. H-bonds involving the amide groups may also enhance mechanical and thermal properties of PEAs compared to the related polyesters, while degradability is still ensured by the presence of labile ester groups.[4,5] In the past years, α-amino acid based PEAs have attracted much attention because they present better biocompatibility than PEAs derived from diamines, as well as the possibility of both hydrolytic and enzymatic degradation.[6,7]

**SCHEME 1: Tautomers of $BAEEH^+$**

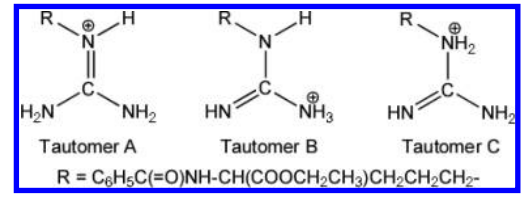


Despite the promising capabilities of PEAs, this type of material has only been studied very scarcely, in particular in what concerns their molecular properties.[8] Evaluation of structure details of simple PEA model compounds may then give a valuable contribution to the understanding of the structure of these systems and provide crucial data for the calibration of better, more efficient, and/or reliable computational methods to be used in the interpretation of complex PEAs.

In this work, the L-arginine derivative, $N_\alpha$-benzoyl-L-argininate ethyl ester chloride ($BAEEH^+ \cdot Cl^-$), a suitable PEA model, was characterized structurally by means of a combined quantum chemistry/$^1$H NMR approach. In theory, the $BAEEH^+$ cation can exist in different tautomeric forms, namely, those characterized by distinct protonation sites in the guanidyl moiety (see Scheme 1). To the best of our knowledge, no studies have been reported on this compound hitherto. In the present study, different tautomers were then investigated theoretically in view of rationalizing the experimental findings. Both theoretical and

* Corresponding author. E-mail: pnsim@eq.uc.pt.
[†] Department of Chemical Engineering.
[‡] Department of Chemistry.
[§] Department of Life Sciences and Center for Neurosciences.

10.1021/jp9114749 
Published on Web 04/16/2010

experimental data give strong evidence that tautomer **A** is the preferred one in the studied media, i.e., gaseous phase and in dimethylformamide solution.

## Materials and Methods

**Computational Details.** Conformational searches on the semiempirical PM3[9,10] potential energy surfaces (PES) of the three lowest-energy tautomers of $BAEEH^+$ shown in Scheme 1 were performed using a stochastic approach based on variation of all conformationally relevant torsion angles,[11] as implemented in the Hyperchem 8.03 program.[12] This allowed the putative most stable conformers of each tautomer to be found, which were subsequently considered in the higher-level density functional theory (DFT) calculations.[13,14] The DFT computations were carried out with the Gaussian03 package[15] using the Becke-style three-parameter with the Lee−Yang−Parr correlation functional (B3LYP).[16−18] The DFT calculations were accomplished by the 6-31++G(d,p) Pople-type basis set[15] after a preliminary scrutiny performed at the DFT(B3LYP)/6-31G(d) level of theory. The 6-31++G(d,p) basis set appeared to be a good compromise for the system under study, as suggested by some performed tests (data not shown), in which only a slight improvement in the results was found on going from a double- to triple-$\zeta$ basis set, 6-311++G(d,p).[15] The molecular geometries were fully optimized by the force gradient method using the Berny algorithm[19] and applying the tight convergence criteria.[15] All these computations were performed for the isolated molecule in vacuo. The nature of the obtained stationary points was checked by vibrational frequency calculations to ensure that the structures were true minima in the PES (this applies to all DFT optimizations here reported).

Accordingly to the experimental part (see below), solvent effects were taken into account in the calculations by using the polarized continuum model (PCM).[20−25] Dimethylformamide [DMF; $(CH_3)_2NC(=O)H$] was used as solvent (since DMF is not available in Gaussian03's PCM method, it was defined according to the following parameters:[26] EPS = 36.71, RSOLV = 2.647, and DENSITY = 0.00778), and the universal force field (UFF) model was applied to build up the molecular cavity. These computations were performed on the six most stable conformers of tautomer **A**, as well as on the stablest conformers of tautomers **B** and **C**. Since PCM does not treat the effect of explicit H-bonding in condensed phase, a supermolecular model based on a $BAEEH^+$−water complex was also used to simulate specific intermolecular H-bonds in solution. The most stable tautomer/conformer of $BAEEH^+$ was chosen for these calculations, and its structure was reoptimized for the considered solvent and for the $BAEEH^+$−water complex (in vacuo) at the same level of theory [DFT(B3LYP)/6-31++G(d,p)].

The $^1H$ NMR spectra for all models were computed also at the DFT(B3LYP)/6-31++G(d,p) level of theory, using the GIAO method[27] as implemented in Gaussian03.

**Experimental Details.** $N_\alpha$-benzoyl-L-argininate ethyl ester chloride ($BAEEH^+ \cdot Cl^-$; purity ≥99.0%) was purchased from Fluka. Prior to the NMR measurements, a sample of the solid compound was placed on a glass Petri dish in a vacuum oven at 25 °C, for one week, to remove residual moisture.

For the $^1H$ NMR studies in liquid solution, it is essential to have a solvent that keeps the liquid physical state in the temperature range studied, and dimethylformamide (DMF) obeys this requisite. $^1H$ NMR spectra of $BAEEH^+ \cdot Cl^-$ in deuterated DMF (DMF-$D_7$), in the temperature range [−55 to 75 °C], were obtained on a Varian Unity 500 MHz spectrometer using a 5 mm broadband NMR probe. Each spectrum consisted of 32 averaged scans, and acquisition parameters included 36k points, covering a spectral width of 6 kHz, a 30° radiofrequency excitation pulse, and a total repetition time between scans of 10 s, to allow full relaxation. Digital zero filling to 64k and a 0.5 Hz exponential were applied before Fourier transformation. Samples were prepared by dissolving 10 mg of $BAEEH^+ \cdot Cl^-$ in 600 $\mu$L of the deuterated solvent.

## Results and Discussion

**Theoretical Calculations.** For each tautomer of $BAEEH^+$ (see Scheme 1) there are 14 different rotation axes that can give rise to conformational isomers. Thus, a huge number of possible conformers should be expected, which makes a strict conformational search a prohibitive task. Our first approach was to perform a conformational search on the PES of these three tautomeric forms at the semiempirical PM3 level of theory, which allowed the identification of up to five tens of local minima within a relative energy range of ca. 10 kJ $mol^{-1}$ for tautomers **A**, **B**, and **C**. From this analysis (Table S1 in the Supporting Information includes structural and energetic data resulting from this analysis), tautomer **A** was predicted to be much more stable than the other tautomers, being more stable than **B** and **C** by ca. 65 and 68 kJ $mol^{-1}$, respectively (considering the PM3 predicted most stable conformer of each tautomer).

The large number of structures with PM3 relative energies up to ca. 10 kJ $mol^{-1}$ would still be very demanding computationally if their full optimization and other properties (vibrational frequencies and chemical shifts) were calculated at higher levels of theory. Thus, the study was restricted to the structures within a PM3 relative energy range of ca. 5 kJ $mol^{-1}$. Under these conditions, 18, 7, and 22 geometries for tautomers **A**, **B**, and **C**, respectively, were used as input geometries in DFT calculations. The first applied DFT(B3LYP)/6-31G(d) optimizations permitted to reduce the number of species under study because some input structures have converged to the same one. These were then studied at the DFT(B3LYP)/6-31++G(d,p) level of theory, leading to six, four, and eight conformers for tautomers **A**, **B**, and **C**, respectively, with relative energies less than ca. 10 kJ $mol^{-1}$ for each tautomer.

The subsequent study was circumscribed in the light of the magnitude of the relative stabilities of the three tautomers. Thus, the six most stable conformers of tautomer **A**, as well as only the most stable forms of tautomers **B** and **C**, were further investigated by means of PCM computations. This theoretical study allowed us to confirm that tautomer **A** is considerably more stable than tautomers **B** and **C**, both in vacuo and in DMF, thus clearly suggesting its actual occurrence in solution instead of the remaining two. Table 1 resumes relevant results of this analysis, and Figure 1 depicts the structures of the studied conformers of tautomer **A**, as well as of the most stable conformers of tautomers **B** and **C**, calculated at the DFT(B3LYP)/6-31++G(d,p) level of theory. As can be seen from Table 1, going from in vacuo to DMF environment, the **A.II** structure is slightly destabilized. However, the remaining conformers of tautomer **A** follow the same energetic trend in both media here investigated. The **B** and **C** tautomers are stabilized in DMF. Nevertheless, the superior relative stability of tautomer **A** in both media is evident.

***Relative Stability of the Conformers of Tautomer A.*** Being the most stable and, with all probability, the one whose actual occurrence should be expected, tautomer **A** deserves to be considered in more detail. The structures of the studied conformers of tautomer **A**, calculated at the DFT(B3LYP)/6-

**TABLE 1: Relative Energies with Zero-Point Energy (ZPE) Correction with Respect to the Most Stable Conformer of Tautomer A and Total Dipole Moments for the Studied BAEEH$^+$ Tautomers/Conformers (see Figure 1) in Vacuo and Dimethylformamide (DMF) Obtained at the DFT(B3LYP)/6-31++G(d,p) Level of Theory**

| | in vacuo | | in solution (DMF) | |
|---|---|---|---|---|
| tautomer. conformer | $\Delta E^{ZPE}$ (kJ mol$^{-1}$)[a] | $\|\mu\|$ (D) | $\Delta E^{ZPE}$ (kJ mol$^{-1}$)[b] | $\|\mu\|$ (D) |
| **A.I** | 0.00 | 10.34 | 0.00 | 13.33 |
| **A.II** | 1.87 | 10.39 | 3.34 | 13.44 |
| **A.III** | 1.92 | 10.40 | 2.58 | 13.45 |
| **A.IV** | 2.44 | 10.48 | 3.12 | 13.41 |
| **A.V** | 5.16 | 10.35 | 3.19 | 13.62 |
| **A.VI** | 10.07 | 8.60 | 9.13 | 10.87 |
| **B** | 164.87 | 6.40 | 136.42 | 9.69 |
| **C** | 102.29 | 4.99 | 98.29 | 6.32 |

[a] The calculated energies in vacuo for the most stable conformers of tautomers **A**, **B**, and **C** of BAEEH$^+$ are, respectively, −1030.06957, −1029.6245, and −1029.64838 au. [b] The calculated energies in DMF for the most stable conformers of tautomers **A**, **B**, and **C** of BAEEH$^+$ are, respectively, −1029.75676, −1029.70480, and −1030.71965 au (additional calculated data on tautomers **B** and **C** can be found in Tables S5−S7 of the Supporting Information).

31++G(d,p) level of theory, are depicted in Figure 1 (see Table 1 for their relative energies and dipole moments). Table 2 presents the conformations adopted by the 14 independent internal rotation axes in each conformer (Table S2 is an extended version of Table 2). The calculated H-bond geometrical parameters are also given in this table. Since there are no noticeable differences between geometries calculated in vacuo and those computed in DMF, for the sake of simplicity only results obtained in vacuo will be considered in what follows.

From Figure 1 it can be seen that tautomer **A** tends to adopt folded structures because these facilitate the establishment of energetically favorable intramolecular interactions, in particular of the H-bond type. All conformers have the carboxylic ester group (O=C−O−R) in the *s-cis* orientation, which is known to be intrinsically more stable than the *s-trans* arrangement,[28,29] and the guanidinium group is planar.[30] The six most stable conformers are stabilized by a bifurcated H-bond involving the carbonyl oxygen atom of the amide linkage and the nitrogen atoms of the protonated guanidinium group, forming a six-membered ring (Figure 1). The H-bond geometrical parameters (Table 1) suggest that the bifurcated H-bond in conformer **A.VI** is weaker than those of the other conformers. The bifurcated H-bond was found to be asymmetric: for all conformers, the N(14)−H···O$_{Amide}$ arm of the bifurcated bond is relatively shorter than the N(16)−H···O$_{Amide}$ one, and the N(14)−H···O angle is less deviated from linearity than the N(16)−H···O$_{Amide}$ angle [conformer **A.VI**: ∠(N(14)−H···O) = 158°, *d*(H···O) = 2.779 Å; remaining conformers: ∠(N(14)−H···O) = 157−161°, *d*(H···O) = 2.731−2.757 Å (Table 1)]. For the five most stable conformers, an additional H-bond-like interaction exists between the carbonyl oxygen of the ester linkage and the N−H$_{Amide}$ group. It gives rise to a five-membered ring and is considerably less strong than the previously referred to six-membered ring H-bonds, as shown by the corresponding H-bond parameters presented in Table 2.

Very interestingly, the *anti* conformation of the ethyl ester group is only observed in the most stable conformer (**A.I**). In the remaining low-energy conformers of BAEEH$^+$, this group adopts the *gauche* (or *gauche′* conformation (Table 2). Indeed, **A.I** differs from **A.III** and **A.IV** only in the conformation of the ester group (Figure 1). These two latter conformers were found to be less stable than **A.I** by ca. 2 kJ mol$^{-1}$. The *anti* conformation of the ester fragment is also the most stable one for example in ethyl acetate.[31] This increased stability of the *anti* arrangement of the C−O$_{Ester}$−C−C dihedral in relation to the *gauche* one has been explained considering that such an arrangement makes the distance between the terminal methyl group and the carbonyl oxygen atom longer, thus minimizing the repulsive destabilizing steric interaction between these groups (see Table 2 for the CH$_3$···O= distance).[31]

In all conformers but **A.V**, the C(10)−C(11)−C(12)−C(13)−N(14)−C(15) fragment adopts the same conformation, i.e., the C(12)−C(13)−N(14)−C(15), C(11)−C(12)−C(13)−N(14), and C(10)−C(11)−C(12)−C(13) dihedrals are in the *anti* (A), *gauche′* (G′), and *skew* (SK) configurations, respectively. On the other hand, in **A.V**, these dihedrals assume the SK, G, and G geometries, respectively. Conformers **A.V** and **A.II** differ only in the orientation of these three dihedrals, showing a difference in energy of ca. 3.3 kJ mol$^{-1}$. The preferred AG′SK configuration allows the guanidinium group to be close to the carbonyl oxygen atom of the amide linkage, facilitating the establishment of a more favorable bifurcated H-bond than that allowed by the SKGG configuration (see Table 2).

The less stable conformer (**A.VI**) differs from the most stable one (**A.I**) in the orientation around the C(19)−C(20) and O$_{Ester}$−C(19) bonds, whose effects regarding structures' relative stabilities were already discussed above, but also in the conformation of the N$_{Amide}$−C−C$_{Ester}$=O fragment. In **A.VI**, this fragment adopts the *anti* conformation, precluding the establishment of the H-bond between the carbonyl oxygen atom of the ester group and the N−H$_{Amide}$ moiety, which provides an additional stabilization in the remaining conformers (Table 1). It is also worth noting that conformers **A.II** and **A.VI** only differ in the orientation of the N$_{Amide}$−C−C$_{Ester}$=O dihedral, with the former being ca. 8 kJ mol$^{-1}$ more stable than the latter, which can be a rough estimation of the energy of the N−H$_{Guanidinium}$···O$_{Amide}$ H-bond in conformers **A.I**−**A.V**.

**$^1$H NMR Spectra of BAEEH$^+$·Cl$^-$.** ***Temperature Effects on Guanidinium Protons.*** $^1$H NMR spectra of BAEEH$^+$·Cl$^-$ in DMF-D$_7$, in the −55 to 75 °C temperature range, were acquired. The chemical shifts of all protons of BAEEH$^+$ in the studied temperature range are shown in Table 3. Figure 2 presents a picture of all the protons' peaks at 25 °C. Figure 3 shows the region of the $^1$H NMR spectra where the features due to the amine (−NH$_2$) protons of the guanidinium moiety are observed (at the different temperatures). The behavior of the proton of the amide linkage and the imine proton of the guanidyl group in the studied temperature range is presented in Figure 4.

The set of experiments performed in this work permitted us to identify the BAEEH$^+$ tautomer **A** in solution. The effects of temperature on the rotational motions within the guanidinium moiety were also investigated. The assignments here proposed were supported by the results provided by a correlation spectroscopy (COSY) experiment (data not shown).

The peaks at 7.68 (c) and 7.78 (d) ppm in the spectrum obtained at −55 °C are attributed to the protons of the N(21)H$_2$ group of the guanidinium moiety (Table 3 and Figure 3). These peaks exhibit similar integration areas and peak intensities (Table 3 and Figure 3). The signal (h) observed at 8.22 ppm should be ascribed to the H(37) proton of the N(16)H$_2$ group. Since the N(16)−H(37) bond is involved in an intramolecular H-bond with the amide oxygen atom [N(16)−H(37)···O$_{Amide}$] (Figure 1), it is expected to appear at higher values of chemical shift, i.e.,

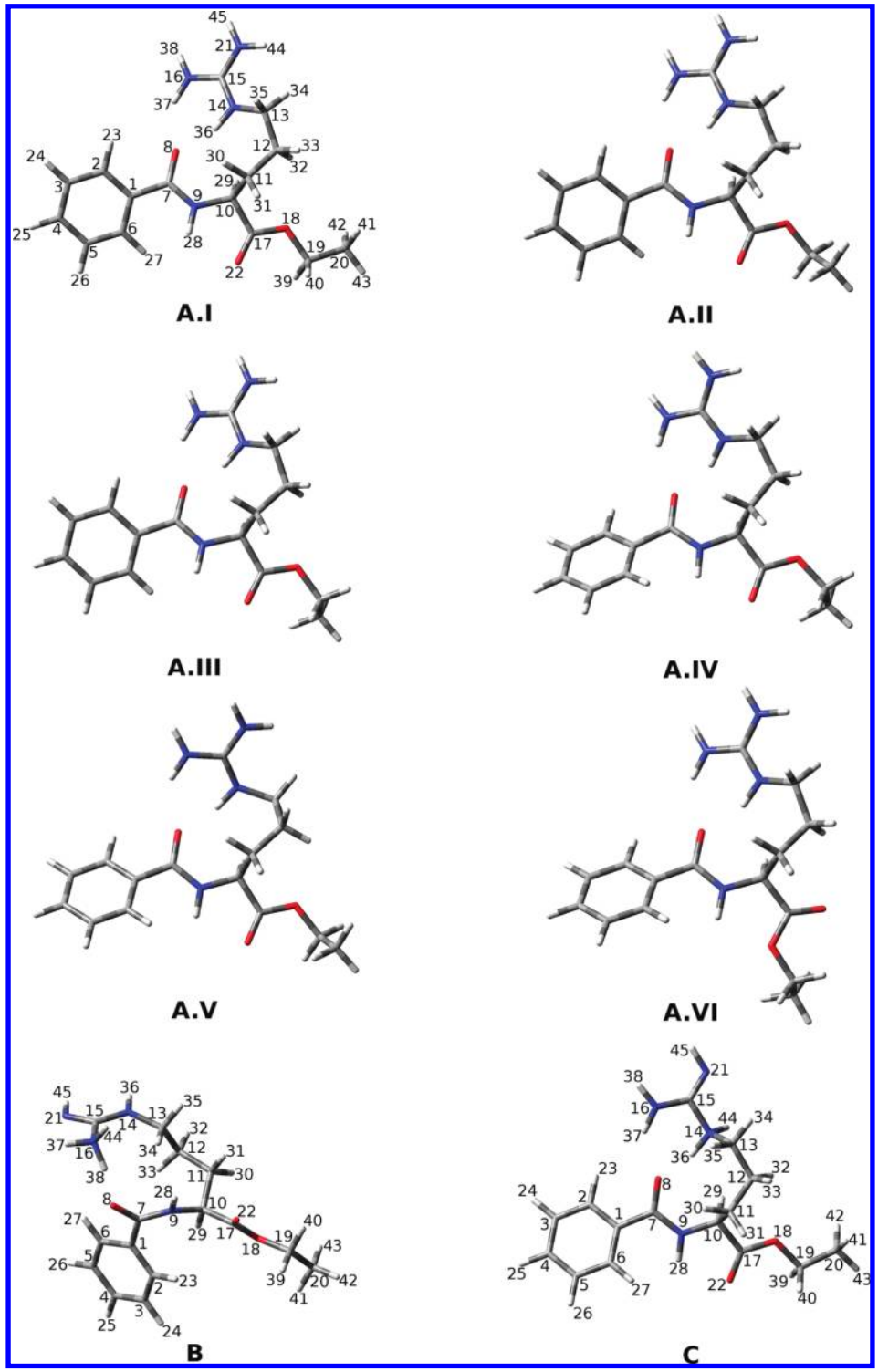


**Figure 1.** Geometries (and atom numbering) of the six most stable conformers of tautomer **A** and the most stable conformers of tautomers **B** and **C** of $BAEEH^+$, obtained at the DFT(B3LYP)/6-31++G(d,p) level of theory in vacuo.

more deshielded than the remaining three amine protons of the guanidinium moiety, which are not involved in an intramolecular H-bond. The (h) peak presents an integration area identical to those of the previously referred protons, (c) and (d) (Table 3). Taking into account this fact, another peak (f) due to the second proton [H(38)] of the $N(16)H_2$ group, with similar integration area, should exist in its proximity. This peak is overlapped with the doublet signal (g) of the *ortho* protons of the phenyl ring (Figure 3).

Upon increasing the temperature to −50 °C, the same peaks are observed, although with a slight change in their absolute chemical shifts compared to those observed at −55 °C (Figure 3). Particularly noticeable is the clear observation at −50 °C of the peak (f) that can now be seen as a shoulder in the lower chemical shifts' wing of the doublet (g). Both at −55 and −50 °C, the four protons of the two amine groups of the guanidinium moiety are nonequivalent, experiencing different chemical environments; i.e., at these temperatures the rotations about the guanidinium C−N bonds occur sufficiently slow to allow signal distinction.[32]

An increase in temperature to −40 °C led to a broadening of the signal of the protons of the $N(21)H_2$ group (Figure 3),

**TABLE 2: Conformations[a] Adopted by the 14 Independent Internal Rotation Axes and Geometrical Parameters of H-Bonds Present in the Conformers of Tautomer A of BAEEH$^+$ (see Figure 1 for Atom Labeling) Obtained at the DFT(B3LYP)/6-31++G(d,p) Level of Theory, in Vacuo and in DMF (in Brackets)**

| | dihedrals[b] | | | | | | | | | | | | | | | | | |
|---|---|---|---|---|---|---|---|---|---|---|---|---|---|---|---|---|---|---|
| | 1 | 2 | 3 | 4 | 5 | 6 | 7 | 8 | 9 | 10 | 11 | 12 | 13 | 14 | $CH_3\cdots O^{=}$[d] (Å) | donor−H···acceptor | donor−H (Å) | H···acceptor (Å) | donor···acceptor (Å) | donor−H···acceptor (°) |
| **A.I** | G | A | S | A | A | S | A | G′ | SK | S | SK′ | G | S | A | 4.19 (4.19) | N(14)−H···$O_{Amide}$ | 1.035 (1.026) | 1.736 (1.819) | 2.732 (2.814) | 160.22 (162.16) |
| | | | | | | | | | | | | | | | | N(16)−H···$O_{Amide}$ | 1.017 (1.013) | 2.056 (2.182) | 2.913 (3.034) | 140.42 (140.62) |
| | | | | | | | | | | | | | | | | $N_{Amide}$−H···$O_{Ester}$ | 1.014 (1.013) | 2.184 (2.262) | 2.652 (2.686) | 106.17 (103.56) |
| **A.II** | G′ | G′ | S | A | A | S | A | G′ | SK | S | SK′ | G | S | A | 3.35 (3.39) | N(14)−H···$O_{Amide}$ | 1.035 (1.027) | 1.733 (1.815) | 2.731 (2.812) | 160.49 (162.98) |
| | | | | | | | | | | | | | | | | N(16)−H···$O_{Amide}$ | 1.017 (1.013) | 2.062 (2.204) | 2.918 (3.053) | 140.20 (140.41) |
| | | | | | | | | | | | | | | | | $N_{Amide}$−H···$O_{Ester}$ | 1.014 (1.013) | 2.183 (2.258) | 2.651 (2.683) | 106.18 (103.58) |
| **A.III**[c] | G | G | S | A | A | S | A | G′ | SK | S | SK′ | G | S | A | 3.35 (3.38) | N(14)−H···$O_{Amide}$ | 1.034 (1.026) | 1.740 (1.822) | 2.735 (2.818) | 160.11 (162.71) |
| | | | | | | | | | | | | | | | | N(16)−H···$O_{Amide}$ | 1.017 (1.013) | 2.055 (2.181) | 2.913 (3.032) | 140.48 (140.49) |
| | | | | | | | | | | | | | | | | $N_{Amide}$−H···$O_{Ester}$ | 1.014 (1.013) | 2.188 (2.265) | 2.653 (2.686) | 105.98 (103.33) |
| **A.IV** | G | G | S | A | A | S | A | G′ | SK | S | SK′ | G | S | A | 3.35 (3.38) | N(14)−H···$O_{Amide}$ | 1.031 (1.025) | 1.778 (1.842) | 2.757 (2.824) | 156.95 (159.36) |
| | | | | | | | | | | | | | | | | N(16)−H···$O_{Amide}$ | 1.019 (1.014) | 2.009 (2.137) | 2.882 (2.999) | 142.16 (141.69) |
| | | | | | | | | | | | | | | | | $N_{Amide}$−H···$O_{Ester}$ | 1.015 (1.013) | 2.155 (2.216) | 2.649 (2.675) | 107.88 (105.79) |
| **A.V** | G′ | G′ | S | A | A | S | SK | G | G | S | SK′ | G | S | A | 3.33 (3.37) | N(14)−H···$O_{Amide}$ | 1.035 (1.026) | 1.736 (1.828) | 2.736 (2.828) | 161.35 (163.78) |
| | | | | | | | | | | | | | | | | N(16)−H···$O_{Amide}$ | 1.018 (1.012) | 2.128 (2.391) | 2.982 (3.205) | 140.24 (136.85) |
| | | | | | | | | | | | | | | | | $N_{Amide}$−H···$O_{Ester}$ | 1.015 (1.013) | 2.151 (2.206) | 2.649 (2.675) | 108.15 (106.41) |
| **A.VI** | G′ | G′ | S | A | A | S | A | G′ | SK | A | SK′ | G | S | A | 3.36 (3.39) | N(14)−H···$O_{Amide}$ | 1.029 (1.024) | 1.798 (1.850) | 2.779 (2.833) | 157.85 (159.83) |
| | | | | | | | | | | | | | | | | N(16)−H···$O_{Amide}$ | 1.018 (1.014) | 2.031 (2.149) | 2.905 (3.011) | 142.40 (141.71) |

[a] S: *Syn* ≅ 0°. G: *Gauche* ≅ 60°. G′: *Gauche′* ≅ −60°. SK: *Skew* ≅ 120°. SK′: *Skew′* ≅ −120°. A: *Anti* ≅ 180°. [b] 1: $O_{Ester}$−C−C−H(41). 2: $C_{Ester}$−O−C−C. 3: $O_{Ester}$=C−O−C. 4: N(21)−C−N(16)−H(37). 5: N(16)−C−N(21)−H(44). 6: C(13)−N(14)−C−N(21). 7: C(12)−C(13)−N(14)−C. 8: C(11)−C(12)−C(13)−N(14). 9: C(10)−C(11)−C(12)−C(13). 10: $N_{Amide}$−C(10)−$C_{Ester}$=O. 11: $N_{Amide}$−C(10)−C(11)−C(12). 12: C(7)−$N_{Amide}$−C(10)−C(11). 13: $O_{Amide}$=C−$N_{Amide}$−$C_1$. 14: C(6)−C(1)−$C_{Amide}$=O. [c] The conformations adopted by the 14 independent dihedrals in **A.III** and **A.IV** are similar, but they are distinct conformers (see Table S2, Supporting Information, for the values of the dihedrals). [d] Distance between the methyl ($-CH_3$) and carbonyl oxygen atom (O=) of the ester fragment.

suggesting a transition from a slow to intermediate exchange regime. It is worth noting that at this temperature the integration area of the triplet of the *para* protons of the benzyl group at 7.63 ppm (b) increases the equivalent to one proton (Table 3), indicating that the signal overlaps with one of the $N(21)H_2$ protons. The signal corresponding to the H(37) proton (h) of the $N(16)H_2$ group suffers a slight change in its chemical shift (from 8.21 ppm, at −50 °C, to 8.15 ppm, at −40 °C; Table 3). The integration area of the doublet of the *ortho* protons (g) decreases the equivalent to one proton (Table 3), indicating that the signal corresponding to the H(38) proton (f) suffers a shift and now is overlapped by the solvent signal (e) (Figure 3).

At −20 °C, the signals of the $N(16)H_2$ protons (f, h) are significantly enlarged, suggesting an intermediate exchange regime. The peak of the $N(21)H_2$ protons (c, d) is significantly narrowed, indicating a transition to intermediate-fast exchange, and overlaps the signal of the *para* protons (see Figure 3 and Table 3 for the integration area values).

At 0 °C, a decrease in the integration area of the *para* protons triplet (b) is observed (Table 3), indicating that the features due to the $N(21)H_2$ protons are no longer overlapped by this signal. Instead, such protons are shifted slightly upfield, and the respective signal is enlarged (under the *meta* proton peaks (a) leading to an increase in the integration area value of these peaks, Figure 3 and Table 3), most probably due to a significant exchange which starts to occur with the $N(16)H_2$ protons. At 10 °C, a slight broadening of each of the peaks due to each pair of the amine protons of the guanidinium moiety is observed (Figure 3), suggesting that, although the slow exchange regime still prevails, there is an increase in the exchange rate between those protons. At 25 °C, the shape of the line (a very broad band) indicates that all four protons, $N(16)H_2$ and $N(21)H_2$, are in an intermediate exchange regime (Figure 3). A distinct narrower single peak ascribable to the four guanidinium protons is observed at 7.58 ppm, when the temperature is raised to 50 °C, while a further narrowing is observed at 75 °C, suggesting a transition from intermediate to fast exchange regimes (Figure 3). At 75 °C, all four protons are chemically and magnetically equivalent. It should be noted that the peak assigned to the four protons of the guanidinium moiety is overlapped by the signal of the *para* protons of the aromatic ring, leading to a substantial increase of its integration area (see Figure 3 and Table 3 for the integration area value).

An upfield shift of the signals as the temperature increases usually indicates a weakening of intramolecular H-bonds in solution.[33] Moreover, the coalescence of the signals due to a fast proton exchange is in accordance with a decrease in the H-bond strength. A dependence of the H-bond strength with temperature can be noticed from the behavior of the proton H(37) of the $N(16)H_2$ group, which is known to be involved in an intramolecular H-bond [N(16)−H(37)···$O_{Amide}$].

It is also worth noting that the temperature does not much affect the position of the peak due to the N−$H_{Imine}$ proton (i) (Figure 4). This behavior suggests that the imine proton is involved in a strong intramolecular H-bond, which is maintained as the temperature is increased to 75 °C. In fact, the DFT(B3LYP)/6-31++G(d,p) calculations predict that in tautomer **A** of BAEEH$^+$ the intramolecular N−$H_{Imine}$···$O_{Amide}$ H-bond is the strongest of the predicted intramolecular H-bonds in the molecule (Table 2). On the other hand, for the N−$H_{Amide}$ proton (j), a shielding effect upon increasing the temperature is observed (Figure 4), which could be attributed to a possible interaction of this proton with residual water molecules that are present in solution. Apparently, there are two proton−acceptor

**TABLE 3: Experimental $^1$H NMR Chemical Shifts (ppm) for BAEEH$^+$·Cl$^-$, in DMF-$D_7$, in the Temperature Range [−55 to 75 °C]**[a]

| | −55 °C | −50 °C | −40 °C | −20 °C | 0 °C | 10 °C | 25 °C | 50 °C | 75 °C |
|---|---|---|---|---|---|---|---|---|---|
| | | | | Amide Proton | | | | | |
| $N-H_{Amide}$ | 9.35 (1)[b] | 9.34 (1) | 9.27 (1) | 9.16 (1) | 8.79 (1) | 9.04 (1) | 8.89 (1) | 8.74 (1) | 8.57 (1) |
| Guanidyl Protons | | | | | | | | | |
| $N-H_{Imine}$ | 8.56 (1.2) | 8.56 (1.1) | 8.55 (1.1) | 8.52 (1.1) | 8.49 (0.9) | 8.48 (1.1) | 8.47 (1.2) | 8.46 (1.2) | 8.43 (1.0) |
| $N(16)H_2/N(21)H_2$ | 8.2[c]; 7.78/7.68 (1.5; 1.5/1.5) | 8.21[c]; 7.76/7.66 (1.4;1.4/1.4) | 8.15[d]; 7.71[e] (1.6;1.5) | 8.10/8.01 [f];7.59 (1.4/0.8) | 7.97; 7.53[g] (2.4) | 7.90[h] (2.3) | 7.81 (4.5) | 7.58 (4.5) | 7.52[i] |
| | | | | Ring Protons | | | | | |
| $C-H_{Ortho}$ | 8.13 (3.7) | 8.14 (4.1) | 8.14 (2.2) | 8.14 (3.0) | 8.12 (2.6) | 8.11 (2.6) | 8.10 (2.6) | 8.08 (2.6) | 8.07 (2.8) |
| $C-H_{Para}$ | 7.63 (1.3) | 7.63 (1.3) | 7.63 (1.8) | 7.58 (3.4) | 7.58 (1.4) | 7.57 (1.9) | 7.57 (2.1) | 7.54 (1.8) | 7.51 (6.4) |
| $C-H_{Meta}$ | 7.56 (2.4) | 7.55 (2.7) | 7.55 (2.2) | 7.53 (2.5) | 7.51 (4.8) | 7.50 (3.5) | 7.50 (2.8) | 7.48 (2.6) | 7.48 (2.5) |
| | | | | Ethyl Ester Protons | | | | | |
| $CH_{2Ester}$ | 4.12 | 4.12 | 4.14 | 4.15 | 4.16 | 4.16 | 4.16 | 4.17 | 4.17 |
| $CH_{3Ester}$ | 1.22 | 1.21 | 1.22 | 1.22 | 1.22 | 1.23 | 1.23 | 1.23 | 1.23 |
| | | | | Carbon Chain Protons | | | | | |
| $C-H_{Methine}$ | 4.46 | 4.46 | 4.48 | 4.50 | 4.52 | 4.52 | 4.55 | 4.58 | 4.58 |
| $C(13)H_2$ | 3.35 | 3.35 | 3.34 | 3.35 | 3.35 | 3.35 | 3.35 | [j] | 3.37 |
| $C(11)H_2$ | 1.99 | 1.99 | 2.00 | 2.00 | 2.02 | 2.02 | 2.03 | 2.03 | 2.05 |
| $C(12)H_2$ | 1.81 | 1.81 | 1.81 | 1.80 | 1.80 | 1.80 | 1.81 | 1.81 | 1.81 |

[a] See Figure 1 for atom labeling. [b] The numbers indicated in brackets correspond to the integration area of the peak. [c] The proton H(38) is overlapped by the signal of the *ortho* protons of the phenyl ring. [d] The proton H(38) is overlapped by the signal of the solvent. [e] One of the $N(21)H_2$ protons is overlapped by the *para* protons of the phenyl ring. [f] Corresponds to the proton H(38). [g] The signal of the protons of the $N(21)H_2$ group is overlapped by the signal of the *meta* proton of the phenyl ring. [h] Broad signal corresponding to the protons $N(16)H_2$ starting to exchange with the $N(21)H_2$. [i] The four protons of the guanidinium moiety are overlapped by the signal of the *para* protons of the phenyl ring. [j] Overlapped by the signal of the water protons.

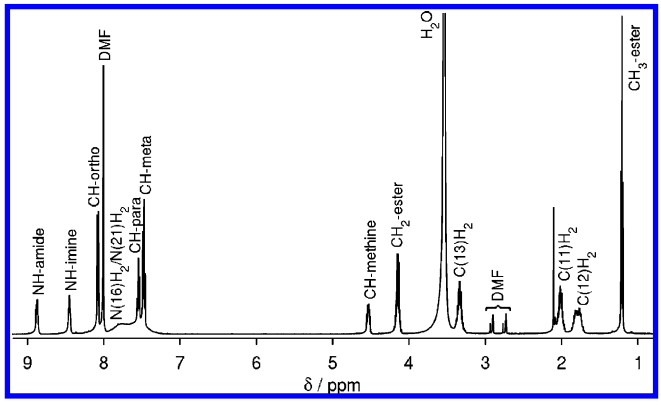


**Figure 2.** $^1$H NMR spectrum of BAEEH$^+$·Cl$^-$, in DMF-$D_7$, at a temperature of 25 °C.

competitors for the amide proton, BAEEH$^+$ ester and water oxygen atoms.

***Experimental versus Theoretical $^1$H NMR Spectra (Room Temperature).*** As previously stated, the predicted relative stabilities of the three plausible BAEEH$^+$ tautomers under study (see Scheme 1) clearly indicate that **A** should be recognized as the actual tautomeric form, at least in the investigated media. Nevertheless, the calculation of DFT(B3LYP)/6-31++G(d,p) $^1$H NMR chemical shifts was extended to all tautomers/conformers presented in Figure 1 (i.e., six conformers of tautomer **A**, as well as tautomers **B** and **C**). These computations were performed both in vacuo and in solution (DMF) using the GIAO method.

The models involving only an isolated BAEEH$^+$ molecule are lacking in describing the effects of possible interactions between a BAEEH$^+$ molecule and its surrounding environment, viz., solvent and/or inevitable residual water molecules. Even the PCM approach, which models the chemical environment surrounding a molecule as a polarizable (continuum) medium, does not describe explicit hydrogen bonds. To circumvent this limitation, an alternative (although also simplified) model based on an optimized **A.I** BAEEH$^+$−water complex (Figure 5) was also used.

Considering first the computed NMR data for tautomer **A**, it was found that the predicted chemical shifts of homologue protons in different conformers are quite similar (complementary data in Tables S3 and S4 of the Supporting Information). Most of the cases are predicted within an interval less than ca. 0.5 ppm, excepting H(39) (1.15 ppm), H(40) (1.15 ppm), and H(36) (0.99 ppm) (see Figure 1 for atom labeling). These results agree with the absence of any dramatic structural difference between the conformers under comparison.

The comparison of the calculated chemical shifts for tautomers **A.I**, **B**, and **C** shows some remarkable differences, particularly in the case of guanidinium protons. Taking the results for **A.I** as reference and starting by analyzing the chemical shifts of protons bonded to carbon atoms, the greatest differences predicted for the species **B** in vacuo are 1.05 and 1.09 ppm for protons H(13) and H(33), respectively, whereas in DMF the differences appear to be attenuated. The computed chemical shifts of C−H protons for tautomer **C** are globally quite close to those predicted for tautomer **A.I** (the most pronounced differences are 0.93 ppm in vacuo and 0.73 in DMF for H(34) in both cases). As far as the chemical shifts of guanidinium protons are concerned, the divergences are much more pronounced. The most dramatic differences correspond to the chemical shifts of guanidinium protons involved in intramolecular H-bonds. In the $^1$H NMR spectrum of the **A.I** tautomer, the most deshielded proton, H(36), which is involved in a $N_{Imine}-H(36)\cdots O=_{Amide}$ H-bond, is predicted to appear at 10.80 ppm in vacuo (9.01 ppm in DMF). However, both $^1$H NMR spectra of **B** and **C** tautomers present signals to a remarkable low field, i.e., more deshielded protons than H(36) of tautomer **A**. In tautomer **B**, the intramolecular H-bond formed between the amide oxygen and the ammonium group, H(38) atom, shifts the resonance of this proton to 15.89 ppm in vacuo (12.39 in DMF). The $^1$H NMR spectrum of tautomer **C** exhibits a signal at 13.57 ppm in vacuo (11.85 in DMF), which

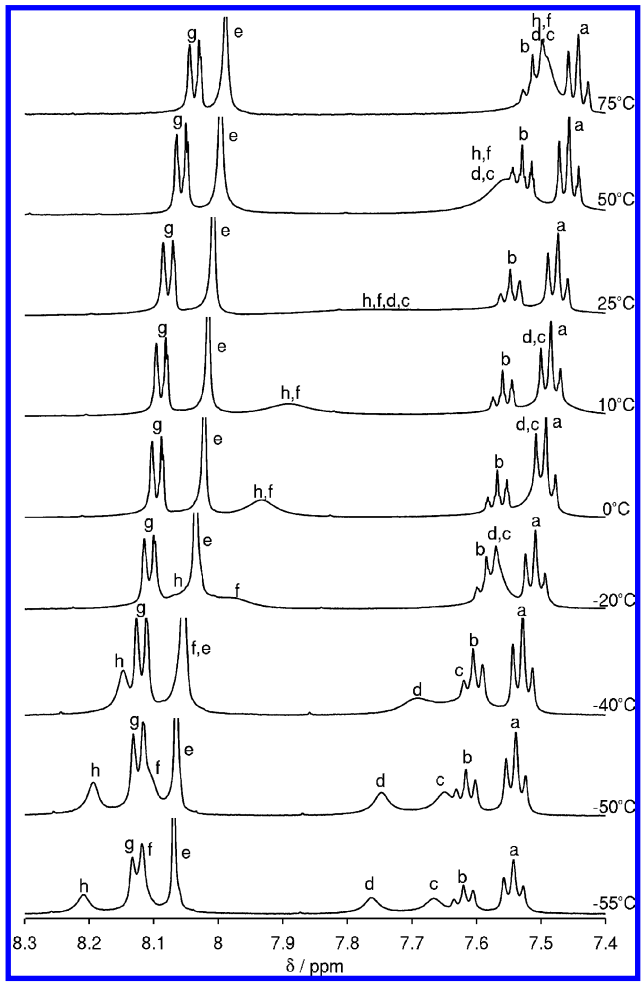


**Figure 3.** $^1$H NMR spectra of BAEEH$^+$·Cl$^-$, in DMF-$D_7$, in a 7.50−8.31 ppm spectral region, acquired at temperatures from −55 to 75 °C. From right to left, letters a−h refer to the following protons: (a) *meta* protons [H(24) and H(26)]; (b) *para* proton [H(25)]; (c,d) the two protons of N(21) [H(44), H(45)]; (e) solvent signal; (f) one of the protons of N(16)$H_2$ [H(37)]; (g) *ortho* protons [H(23) and H(27)]; (h) the other proton of N(16)$H_2$ [H(38)].

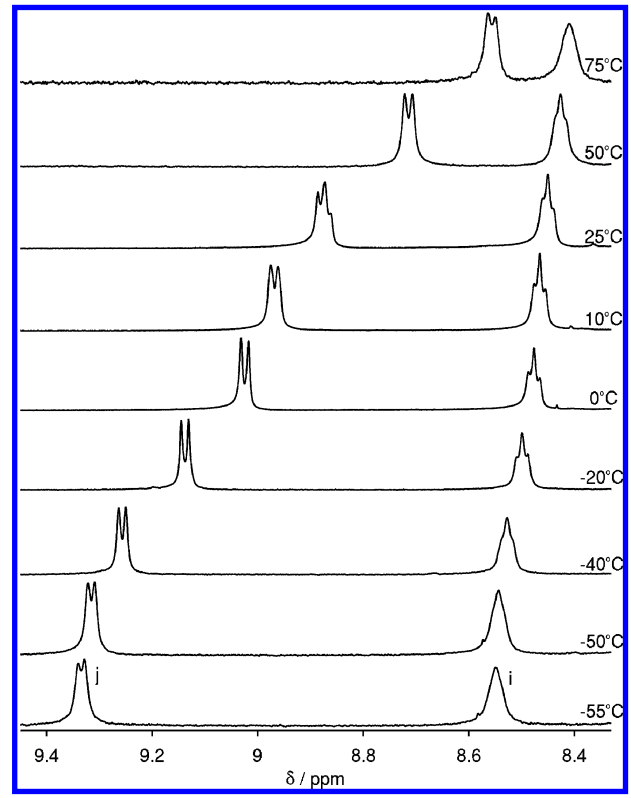


**Figure 4.** $^1$H NMR spectra of BAEEH$^+$·Cl$^-$, in DMF-$D_7$, in a 8.35−9.60 ppm spectral region, acquired at temperatures from −55 to 75 °C. Letters i and j refer to the following protons: (i) $NH_{Imine}$ [H(36)]; (j) $NH_{Amide}$ [H(28)].

corresponds to the proton H(36), involved in a N(14)−H(36)···O=$_{Amide}$ H-bond. Since tautomers **B** and **C** resonate at significantly different chemical shifts when compared with tautomer **A**, these differences should be experimentally revealed, provided that a detectable quantity of each tautomer is present in solution.

Table 4 summarizes the experimental and the DFT(B3LYP)/6-31++G(d,p) calculated $^1$H NMR chemical shifts for the most stable conformers of tautomers **A**, **B**, and **C** of BAEEH$^+$. The C−H proton chemical shifts are notably well explained by the calculated values for the three tautomers. The agreement between the computed and the experimental data is within narrow intervals, the differences being less than 0.80 ppm (except one case H(29), corresponding to 1.06 ppm) for the calculations performed in vacuo and even less in DMF. On the other hand, as anticipated above, the calculated chemical shifts for the guanidinium protons, mainly those involved in intramolecular H-bonds, permit a clear distinction between the tautomers. The most representative cases correspond to the chemical shifts of proton H(38) in tautomer **B** (differences between experimental and computed values of 8.06 and 4.58 ppm in vacuo and DMF, respectively) and of proton H(36) in tautomer **C** (differences between experimental and computed values of 5.10 and 3.38 ppm in vacuo and DMF, respectively).

Focusing now the discussion on tautomer **A**, the main discrepancy between experimental and calculated data for isolated BAEEH$^+$ corresponds to the NH protons not involved in intramolecular H-bonds. This divergence can be related with the possible interactions established between BAEEH$^+$ and the solvent, not accounted for in the theoretical calculations for the isolated molecule in vacuo. As can be seen from Table 4, the improvement in the predicted chemical shifts of (most) CH protons when the study in vacuo is replaced by the PCM or the BAEEH$^+$−water model is limited, and a few cases are even slightly worse. This is not very critical because the calculated values in vacuo for this type of proton are rather satisfactory. On the contrary, the PCM scheme exhibits quite modest results regarding the guanidinium group. Despite the slight change in the calculated chemical shifts of the guanidinium group protons due to the inclusion of the solvent in these calculations, the discrepancy between the computed and experimental values remains considerable. On the other hand, the model based on the BAEEH$^+$−water complex leads to clearly improved results, indicating that it accounts in a fairly good way for the behavior of the title compound in solution. This result clearly confirms that the guanidinium group of BAEEH$^+$ is prone to establish interactions in solution, most probably by means of intermolecular H-bonds with the solvent and/or unavoidable residual water molecules.

To conclude, it should be evoked here that owing to the noticeable differences in the predicted stabilities of tautomers **B** and **C** relative to tautomer **A** (see Table 1) the latter is by far the most probable (in vacuo and in DMF). Putting the predicted data (relative stabilities and $^1$H NMR spectra) together with the experimental findings, which show that the chemical shifts, both in number and quality, correspond to a single tautomer, it is concluded that this must be tautomer **A**. In fact, all resonances

**TABLE 4: Comparison between the Experimental ($T$ = 25 °C) and Theoretical [GIAO; DFT(B3LYP)/6-31++G(d,p)] $^1$H NMR Chemical Shifts (ppm) for the BAEEH$^+$·Cl$^-$ Compound[a]**

| | | theoretical | | | | | | |
|---|---|---|---|---|---|---|---|---|
| | experimental | **A.I** | **A.I** (PCM) | **I.A** (+4$H_2O$) | **B** | **B** (PCM) | **C** | **C** (PCM) |
| | | | | Amide Proton | | | | |
| N−$H_{Amide}$ | 8.89 | 7.81 | 7.69 | 9.80 | 5.86 | 5.85 | 8.04 | 7.94 |
| | | | | Guanidyl Protons | | | | |
| N−$H_{Imine}$ | 8.47 | 10.80 | 9.01 | 9.66 | 3.90 | 4.59 | 13.57 | 11.85 |
| N(16)$H_2$/N(21)$H_2$ | 7.81 | 4.60/4.51; 7.35/4.38 | 5.85/5.43; 6.32/5.79 | 8.73/7.39; 6.65/6.17 | 15.87/5.36; 7.35/4.76 | 12.39/5.47; 6.71/5.74 | 6.49/4.26; 7.63/4.44 | 6.73/4.78; 7.16/5.01 |
| | | | | Ring Protons | | | | |
| C−$H_{Ortho}$ | 8.10 | 7.63 | 8.24 | 8.58 | 7.89 | 7.89 | 8.02 | 8.18 |
| C−$H_{Para}$ | 7.57 | 8.05 | 8.17 | 7.87 | 8.12 | 8.01 | 8.23 | 8.09 |
| C−$H_{Meta}$ | 7.50 | 7.90 | 8.11 | 7.80 | 7.90 | 7.84 | 7.89 | 7.88 |
| | | | | Ethyl Ester Protons | | | | |
| $CH_{2Ester}$ | 4.16 | 4.70 | 4.46 | 4.40 | 4.43 | 4.34 | 4.53 | 4.42 |
| $CH_{3Ester}$ | 1.23 | 0.98 | 1.45 | 1.47 | 1.46 | 1.37 | 1.52 | 1.46 |
| | | | | Carbon Chain Protons | | | | |
| C−$H_{Methine}$ | 4.55 | 4.01 | 4.68 | 4.68 | 4.47 | 4.33 | 3.49 | 3.98 |
| C(13)$H_2$ | 3.35 | 3.16 | 3.33 | 3.55 | 3.02 | 3.19 | 3.72 | 3.73 |
| C(11)$H_2$ | 2.03 | 2.41 | 2.11 | 1.97 | 1.63 | 1.74 | 2.06 | 2.13 |
| C(12)$H_2$ | 1.81 | 2.22 | 1.99 | 1.94 | 1.37 | 1.49 | 2.21 | 2.25 |

[a] Theoretical models are: isolated tautomers in vacuo; isolated tautomers in DMF solution (PCM); and a BAEEH$^+$−water complex in vacuo.

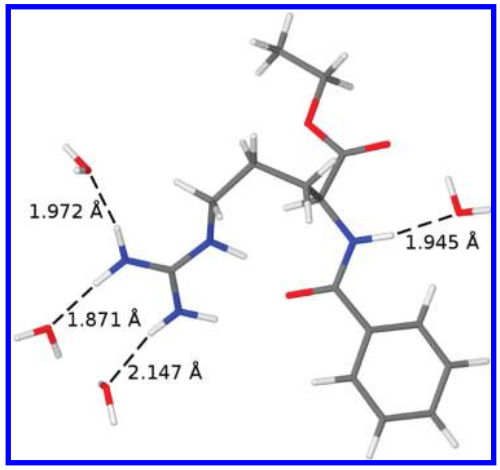


**Figure 5.** Optimized geometry [DFT(B3LYP)/6-31++G(d,p)] of an **A.I** BAEEH$^+$−water complex used to model the possible intermolecular H-bond interactions involving the guanidinium and amide protons (calculation performed in vacuo).

in the experimental $^1$H NMR spectra for all temperatures analyzed were fully assigned to a single tautomer (tautomer **A**). From a practical point of view, either tautomers **B** and **C** are totally absent or their quantities are too small to be detectable by $^1$H NMR spectroscopy. Of course, some of the resonances of tautomer **A** and tautomers **B** and **C** are expected to essentially coincide (as was predicted), but that is not true for some others, such as those mentioned above. In no circumstances were any other resonances at high parts per million values (lower field) consistent with the presence of any significant quantities of tautomers **B** and **C** detected.

## Conclusions

In this work, theoretical (DFT) and experimental ($^1$H NMR spectroscopy) approaches allowed us to investigate the energetic, structural, and spectroscopic properties of an L-arginine derivative, BAEEH$^+$·Cl$^-$, which is a suitable model for PEAs. The data provided in this work thus represent a valuable tool to get new insights about the behavior of more complex systems with similar structure, namely, PEAs.

The DFT(B3LYP)/6-31++G(d,p) calculations carried out on the three BAEEH$^+$ tautomeric forms (Scheme 1) showed that all the lowest-energy conformers for the three tautomers present a folded structure, stabilized by H-bonds between the guanidinium group and the amide carbonyl oxygen atom.

The tautomeric form of BAEEH$^+$ in solution, tautomer **A**, could be successfully identified based on both the theoretical calculations and on $^1$H NMR experiments. The latter also provided detailed information on the intermolecular rotational dynamics of the guanidinium group of the molecule in solution and relative strengths of intramolecular H-bonds.

**Acknowledgment.** A. C. Fonseca acknowledges "Fundação para a Ciência e Tecnologia", Grant: SFRH/BD/41305/2007. S. Jarmelo acknowledges "Fundação para a Ciência e Tecnologia", Grant: SFRH/BPD/22410/2005.

**Supporting Information Available:** Tables of computed relative energies, geometrical parameters, and $^1$H NMR data. Figures of optimized structures. This material is available free of charge via the Internet at http://pubs.acs.org.

## References and Notes

(1) D'Angelo, S.; Galletti, P.; Maglio, G.; Malinconico, M.; Morelli, P.; Palumbo, R.; Vignola, M. C. *Polymer* **2001**, *42*, 3383.
(2) Kajiyama, T.; Taguchi, T.; Kobayashi, H.; Kataoka, K.; Tanaka, J. *Polym. Degrad. Stab.* **2003**, *81*, 525.
(3) Lee, J. W.; Gardella, J. A. *Anal. Bioanal. Chem.* **2002**, *373*, 526.
(4) De Wit, M. A.; Wang, Z. X.; Atkins, K. M.; Mequanint, K.; Gillies, E. R. *J. Polym. Sci., Part A: Polym. Chem.* **2008**, *46*, 6376.
(5) Atkins, K. M.; Lopez, D.; Knight, D. K.; Mequanint, K.; Gillies, E. R. *J. Polym. Sci., Part A: Polym. Chem.* **2009**, *47*, 3757.
(6) Guo, K.; Chu, C. C. *J. Polym. Sci., Part A: Polym. Chem.* **2007**, *45*, 1595.
(7) Guo, K.; Chu, C. C. *Biomacromolecules* **2007**, *8*, 2851.
(8) Casas, M. T.; Puiggali, J. *J. Polym. Sci., Part B: Polym. Phys.* **2009**, *47*, 194.
(9) Stewart, J. J. P. *J. Comput. Chem.* **1989**, *10*, 209.
(10) Stewart, J. J. P. *J. Comput. Chem.* **1989**, *10*, 221.
(11) Chang, G.; Guida, W. C.; Still, W. C. *J. Am. Chem. Soc.* **1989**, *111*, 4379.
(12) HyperChem 8.03. In *HyperChem 8.03*.
(13) Neumann, R.; Nobes, R. H.; Handy, N. C. *Mol. Phys.* **1996**, *87*, 1.

(14) Parr, R.; Wang, W. *Density-Functional Theory of Atoms and Molecules*; Oxford University Press: New York, 1994.

(15) Frisch, M. J.; Trucks, G. W.; Schlegel, H. B.; Scuseria, G. E.; Robb, M. A.; Cheeseman, J. R.; Montgomery, J., J. A.; Vreven, T.; Kudin, K. N.; Burant, J. C.; Millam, J. M.; Iyengar, S. S.; Tomasi, J.; Barone, V.; Mennucci, B.; Cossi, M.; Scalmani, G.; Rega, N.; Petersson, G. A.; Nakatsuji, H.; Hada, M.; Ehara, M.; Toyota, K.; Fukuda, R.; Hasegawa, J.; Ishida, M.; Nakajima, T.; Honda, Y.; Kitao, O.; Nakai, H.; Klene, M.; Li, X.; Knox, J. E.; Hratchian, H. P.; Cross, J. B.; Bakken, V.; Adamo, C.; Jaramillo, J.; Gomperts, R.; Stratmann, R. E.; Yazyev, O.; Austin, A. J.; Cammi, R.; Pomelli, C.; Ochterski, J. W.; Ayala, P. Y.; Morokuma, K.; Voth, G. A.; Salvador, P.; Dannenberg, J. J.; Zakrzewski, V. G.; Dapprich, S.; Daniels, A. D.; Strain, M. C.; Farkas, O.; Malick, D. K.; Rabuck, A. D.; Raghavachari, K.; Foresman, J. B.; Ortiz, J. V.; Cui, Q.; Baboul, A. G.; Clifford, S.; Cioslowski, J.; Stefanov, B. B.; Liu, G.; Liashenko, A.; Piskorz, P.; Komaromi, I.; Martin, R. L.; Fox, D. J.; Keith, T.; Al-Laham, M. A.; Peng, C. Y.; Nanayakkara, A.; Challacombe, M.; Gill, P. M. W.; Johnson, B.; Chen, W.; Wong, M. W.; Gonzalez, C.; Pople, J. A. *Gaussian 03* (revision D.01); Gaussian, Inc.: Wallingford CT, 2004.

(16) Becke, A. D. *Phys. Rev. A* **1988**, *38*, 3098.

(17) Becke, A. D. *J. Chem. Phys.* **1993**, *98*, 5648.

(18) Lee, C. T.; Yang, W. T.; Parr, R. G. *Phys. Rev. B* **1988**, *37*, 785.

(19) Peng, C. Y.; Ayala, P. Y.; Schlegel, H. B.; Frisch, M. J. *J. Comput. Chem.* **1996**, *17*, 49.

(20) Scalmani, G.; Barone, V.; Kudin, K. N.; Pomelli, C. S.; Scuseria, G. E.; Frisch, M. J. *Theor. Chem. Acc.* **2004**, *111*, 90.

(21) Cossi, M.; Rega, N.; Scalmani, G.; Barone, V. *J. Comput. Chem.* **2003**, *24*, 669.

(22) Cossi, M.; Scalmani, G.; Rega, N.; Barone, V. *J. Chem. Phys.* **2002**, *117*, 43.

(23) Cossi, M.; Rega, N.; Scalmani, G.; Barone, V. *J. Chem. Phys.* **2001**, *114*, 5691.

(24) Mennucci, B.; Cances, E.; Tomasi, J. *J. Phys. Chem. B* **1997**, *101*, 10506.

(25) Mennucci, B.; Tomasi, J. *J. Chem. Phys.* **1997**, *106*, 5151.

(26) Boes, E. S.; Livotto, P. R.; Stassen, H. *Chem. Phys.* **2006**, *331*, 142.

(27) Wolinski, K.; Hinton, J. F.; Pulay, P. *J. Am. Chem. Soc.* **1990**, *112*, 8251.

(28) Fausto, R.; de Carvalho, L. A. E. B.; Teixeira-Dias, J. J. C.; Ramos, M. N. *J. Chem. Soc., Faraday Trans. I* **1989**, *85*, 1945.

(29) Fausto, R.; Teixeira-Dias, J. J. C. *J. Mol. Struct.* **1986**, *144*, 241.

(30) Drozd, M. *Spectrochim. Acta Part A-Mol. Biomol. Spectrosc.* **2008**, *69*, 1223.

(31) Fausto, R.; de Carvalho, L. A. E. B.; Teixeira-Dias, J. J. C. *J. Comput. Chem.* **1992**, *13*, 799.

(32) Smith, R. J.; Williams, D. H.; James, K. *J. Chem. Soc., Chem. Commun.* **1989**, 682.

(33) Ash, E. L.; Sudmeier, J. L.; Day, R. M.; Vincent, M.; Torchilin, E. V.; Haddad, K. C.; Bradshaw, E. M.; Sanford, D. G.; Bachovchin, W. W. *Proc. Natl. Acad. Sci. U.S.A.* **2000**, *97*, 10371.

JP9114749